Parametric investigations of a nonconventional Hall thruster*

Y. Raitses† and N. J. Fisch
Princeton Plasma Physics Laboratory, Princeton University, P.O. Box 451, Princeton, New Jersey 08543

(Received 1 November 2000; accepted 22 January 2001)

Hall thrusters might better scale to low power with nonconventional geometry. A 9 cm cylindrical, ceramic-channel, Hall thruster with a cusp-type magnetic field distribution has been investigated. It exhibits discharge characteristics similar to conventional coaxial Hall thrusters, but does not expose as much channel surface. Significantly, its operation is not accompanied by large amplitude discharge low frequency oscillations. © *2001 American Institute of Physics.*
[DOI: 10.1063/1.1355318]

I. INTRODUCTION

In a conventional Hall thruster, axial electric and radial magnetic fields are applied in an annular channel. The magnetic field is large enough to magnetize the electrons, but small enough to leave the ion motion in the channel almost not affected. The magnetic field lines form equipotential surfaces. Electrons experience $E \times B$ flow in the azimuthal direction. The thrust is generated in reaction to the electrostatic acceleration of ions. The ions are accelerated in a quasineutral plasma, so there is no space charge limitation on current and thrust densities.

The ion production can be sustained by a separate ionization source or by impact ionization of propellant atoms injected directly into the channel. For a single-stage conventional Hall thruster, the electrons can gain thermal energy sufficient for ionization by diffusing towards the anode. Acquiring a relatively high electron temperature (10–20 eV), they can also escape along the magnetic field lines.[1] The use of concave magnetic field lines might reduce this defocusing effect on the ion flux.[1,2] Indeed, mostly through optimization of the magnetic field profile, state-of-the-art Hall thrusters now operate with efficiencies (the ratio of the jet power to the input electric power) 50–60 % and thrust densities larger than space-charge-limited ion engines.[1–3]

Larger thrust density leads to a more compact and lighter thruster. At a given ion jet velocity, the thrust is mainly determined by the propellant flow. This flow is almost completely ionized in the Hall thruster channel. Since the momentum is carried by electron current $J_\theta \times B_r$, but $J_\theta = \nabla \times B_r / \mu$, a theoretical limitation for the thrust density of Hall thrusters is roughly equal to the magnetic pressure, $B_m^2/2\mu$.[4] Here, B_m is the maximum magnetic field applied in the channel. For current Hall thrusters, operating in the power range of 0.5–10 kW with $B_m \sim 0.01-0.03$ T, the thrust density is about 20–50 N/m^2, compared to the theoretical limit of about 100–400 N/m^2. Both electron collisions and scattering on oscillations, might produce electron current losses and large beam divergence. Higher power thrusters ($>$0.5 kW) generally maintain the ratio of the gas flow rate to the channel cross sectional area (atomic density).[3] The Hall parameter is then also constant, so that with the same magnetic fields, the thrust density should remain about constant at a given discharge voltage.

However, in scaling to low power thrusters, a simple linear scaling of the overall thruster dimensions leads to potentially higher thrust density than the above scaling approach. To preserve the Hall parameter, the magnetic field is then inversely proportional to the thruster dimensions, increasing the theoretical limit for the thrust density for small thrusters. This linear scaling approach was taken for Hall thrusters designed for 50–200 W power levels.[5] However, lower efficiencies (6% at 100–200 W) were obtained with low power Hall thrusters. The low efficiency might arise from a large axial electron current, enhanced by electron collisions with the channel walls. These results raise doubts about the usefulness of simply miniaturizing the conventional Hall thruster.

Consider instead a cylindrical Hall thruster configuration with a cusp-type magnetic field distribution. The ratio of surface area to volume is reduced, and so might be the wall enhancement of the electron transport and ion losses. It is the object of this paper to examine the attractiveness of this approach.

The paper is organized as follows: In Sec. II we present the scaling arguments for the conventional annular Hall thruster that motivate a new approach at low power. In Sec. III the cylindrical approach to Hall thrusters is described. The present study was facilitated with a laboratory cylindrical thruster of relatively large sizes suitable for a kilowatt power level. In Sec. IV we review the issues in the key diagnostics for Hall thrusters. Section V briefly describes the experimental procedure. Use of a relatively large laboratory thruster and fast movable emissive probe enabled to measure plasma potential profiles with almost no probe induced perturbations in the cylindrical channel. The key experimental results obtained with a cylindrical geometry thruster are described in Sec. VI. In addition to local plasma parameters, the results include integral characteristics as well as the effect of the magnetic field distribution on the thruster operation and its stability. In addition, they are compared to a coaxial Hall thruster of similar sizes with state-of-the-art performance. In Sec. VII we summarize our main conclusions.

*Paper BI2 1, Bull. Am. Phys. Soc. **45**, 19 (2000).
†Invited speaker.

II. LOW POWER SCALING OF ANNULAR HALL THRUSTERS

In scaling the conventional to low power levels, assume constant thruster efficiency. The Hall thruster efficiency can be set as

$$\eta_T = T^2/2\dot{m}P_e \approx \frac{I_i M_i}{e\dot{m}}\frac{I_i}{I_d}\frac{V_{acl}}{V_d},$$

where I_1 is the ion current with kinetic energy eV_{acl}; $T \sim I_1(V_{acl})^{1/2}$ is the thrust, $\dot{m}$ is the mass flow rate, $P_e = I_d V_d$ is the input power; and I_d and V_d are the discharge current and discharge voltage, respectively.[6] The first ratio, $\eta_P = I_e M_i/e\dot{m}$, where M_i is the ion mass, is called propellant utilization. It reflects ion production and ion losses in the channel. The current utilization, $\eta_i = I_i/I_d$ is limited by the axial electron current, J_{ez}, across the magnetic field, since $I_d = I_i + I_{ez}$. The third ratio is the fraction of the energy invested directly to the ion acceleration.

In an efficient thruster, the electron current is much smaller than the ion current at the thruster exit. The input power is then determined by the mass flow rate $P_e \propto \dot{m}V_d$. Hence, low power operation of the Hall thruster with a given jet velocity can be achieved simply by reducing the flow rate of the propellant gas. But such a reduction can affect both the propellant and current utilization.[7]

A simplified equation of the ion flux can give rough scaling relations. We write the ion steady state flux as

$$\frac{\partial J_i}{\partial z} = en_a\nu_a/\lambda_{\text{ion}} - (1-\gamma)\langle J_{er}\rangle/b, \tag{1}$$

where n_e is the atomic densities, γ is the secondary electron emission yield of the channel wall material, λ_{ion} is the ionization mean free path, and b is the channel height. The first term represents impact ionization along the channel producing ions at the gas velocity, ν_a. The second term balances the radial loss of ions to the wall to the loss of electrons to wall, to keep the dielectric wall from charging. It can be approximated as $\alpha J_i/b$, where α is the ratio of the radial and axial ion velocities along the channel. Using Eq. (1) together with mass conservation and current continuity equations, the radial diffusion term in (1), and assuming for simplicity all coefficients, we obtain propellant utilization[7] and current utilization coefficients

$$\eta_p \approx \frac{1}{1+\dfrac{\alpha\lambda_{\text{ion}}}{b}}\left\{1-\exp\left[-L\left(\frac{\alpha}{b}+\frac{1}{\lambda_{\text{ion}}}\right)\right]\right\},$$

$$\eta_I \approx \frac{1}{1+\dfrac{\alpha\lambda_{\text{eff}}}{b}}\left\{1-\exp\left[-L\left(\frac{\alpha}{b}+\frac{1}{\lambda_{\text{eff}}}\right)\right]\right\}, \tag{2}$$

where $\lambda_{\text{eff}} \approx V_d\nu_t/\omega_e BL\nu_{\text{ion}}$ is an effective length associated with the acceleration region, where ω_e is the electron cyclotron frequency and ν_{ion} is the frequency of ionizing collisions.

Assuming that the radial component of the ion velocity arises from the radial electron pressure gradient, the ratio of the radial electric field to the axial electric field is proportional to b/L. Thus, ions leaving the channel without hitting the walls then have $\alpha < b/L$. According Ref. 1, $\lambda_{\text{ion}} \propto \dot{m}^{-2}L^{-1}$. Then, assuming we want to preserve the ionization probability in the channel, which means $\lambda_{\text{ion}}/L \propto 1/(\dot{m}L)^2 \sim$ constant, the propellant utilization is unchanged if $b/L \sim$ constant. Similarly, current utilization is left unchanged if the magnetic field scales as $B \sim 1/L = 1/b$. In this case, the scaling of the overall thruster geometry, plasma, and thruster integral parameters is linear.

Of course, there are many physical effects that will interfere with this simple scaling. Note, that equations (2) do not exhibit the effects of optimizations, such as details of the magnetic field profile. In fact, because of collisionless plasma instabilities, the optimum magnetic field apparently has a minimum near the anode and maximum at the exit.[1,2,8] The effective acceleration region is then smaller than the total channel length. To preserve these optimal profiles in small Hall thrusters is, however, technically challenging.[2,10]

The magnetic circuit, comprising a low carbon core and electromagnetic coils, produces the magnetic field in Hall thrusters. Even in large Hall thrusters, certain narrow parts of the circuit are near saturation ($\approx$15 kG).[10] Apparently, a linear scaling down of the magnetic circuit leaves almost no room for the use of magnetic screens and thin magnetic poles, or for heat shields, making difficult the achievement of the optimal magnetic field profiles.[5,10] Yet nonoptimal magnetic fields will result in enhanced power and ion losses, heating and erosion of thruster parts, particularly the critical inner parts of the coaxial channel and magnetic circuit. Thus, the main obstacle in making a miniaturized conventional thruster is making a practical magnetic circuit.

Miniaturization is made easier by eliminating the thruster inner parts, which is an approach taken in the end-Hall thruster,[9,11] and in a linear Hall-type thruster.[12] The end-Hall thruster preserves closed electron drifts, while in the linear thruster, electron trajectories are closed on ceramic walls. However, all these attempts at miniaturization exhibited significant electron transport across the magnetic field, just as does the conventional small Hall thruster.

III. CYLINDRICAL HALL THRUSTER

The approach we take, what we call a cylindrical Hall thruster, is illustrated in Fig. 1. The thruster consists of cylindrical ceramic channel, ring-shaped anode, which can also be a gas distributor, the magnetic core and magnetized sources. The magnetic field lines intersect the ceramic channel walls. The electron drifts are closed, with the magnetic field lines forming equipotential surfaces, with $E = -v_e \times B$. The radial component of the magnetic field crossed with the azimuthal electron current produces the thrust.

Two magnetized sources, electromagnetic coils with opposite currents, can produce a cusp-type magnetic field in the channel, with a strong radial component. Here, the gas inlet is off-axis to decouple it from the anode and cathode potential surfaces. To maintain ionizing collisions, both the anode and gas inlet are placed in the short coaxial part of the channel. The length of the coaxial channel is selected so that to minimize λ_{ion}/L and thus, to localize the ionization of the

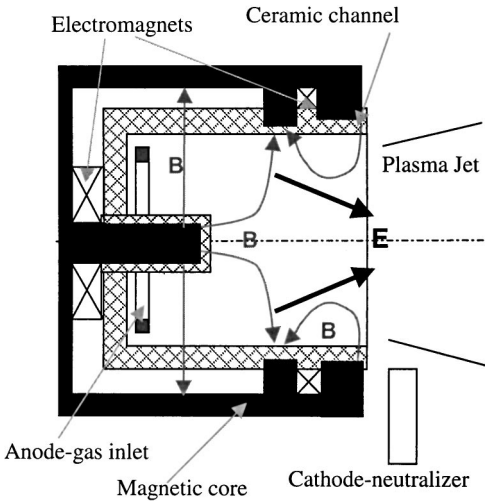

FIG. 1. Principle of operation of the cylindrical Hall thruster.

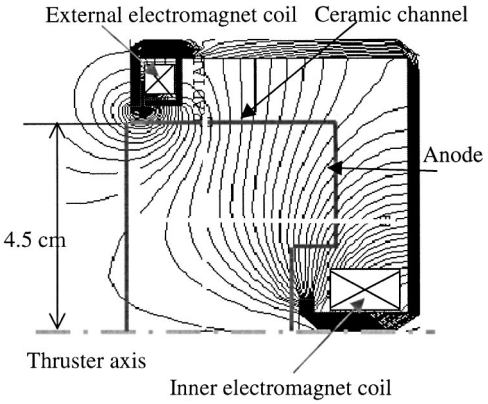

FIG. 3. Magnetic field simulations of the laboratory thruster.

working gas at the boundary of coaxial and cylindrical regions. In this case, the most of voltage drop occurs in the cylindrical region with a larger b/L ratio. This should produce high propellant and current utilization efficiencies [see Eq. (2)].

What distinguishes this thruster from conventional annular and end-Hall thrusters is the cylindrical configuration with an enhanced radial component of the magnetic field. Also, the use of ceramic walls reduces the defocusing effect of the electron pressure. All the advantages of closed electron trajectories are retained.

A 9 cm laboratory cylindrical Hall thruster is shown in Fig. 2. The thruster channel is made from a boron nitride ceramic. The total channel length taken from the anode to the thruster exit is 4 cm with the coaxial part of 1 cm long. The anode serves also as a gas distributor. A commercial Heat-Wave plasma source is used as a cathode neutralizer. The magnetic circuit consists of two coils connected to separate power supplies of opposite polarity. Figures 3 and 4 show the results of magnetic field simulations and measured profile of the magnetic field. The maximum of the radial magnetic field is somewhere near the boundary of the coaxial and cylindrical parts of the channel. However, near the inner wall, there are two maximums of the magnetic field affected by the opposite direction of the currents in the coils and use of a small inner pole (Figs. 3 and 4). In principle, the movable anode can be placed at the edge of the coaxial region to construct a purely cylindrical channel. However, azimuthal waves may be unstable for $\partial(B/n)\partial z<0$.[1]

Note that the axial component of the magnetic field in the cylindrical thruster, near the center line, in particular, should create an electric field distribution similar to some sort of a virtual hollow anode, impeding the ions from reaching the walls. Similar to Refs. 13–15 with coaxial thruster, the use of segmented electrodes may be useful to control the electric field in this particular region of the cylindrical thruster as well.

The thruster experiments took place in a 28 m^3 vacuum vessel equipped with a 35″ diffusion pump and mechanical roots pump. At a xenon gas flow rate of 17 sccm, the measured background pressure was about 17 μtorr that corresponds to the pumping speed of 12 000 l/s for xenon. A research grade xenon gas was supplied to both thruster and cathode. Gas flow rates were measured with two Millipore FC-260 controllers, which, in addition to a manufacturer, were periodically calibrated during the experiments by a volumetric method. The main thruster discharge was supported by a 1 kV dc voltage regulated switching power sup-

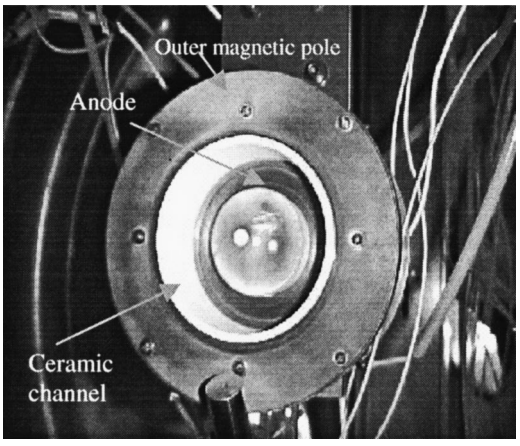

FIG. 2. A 9 cm laboratory cylindrical Hall thruster.

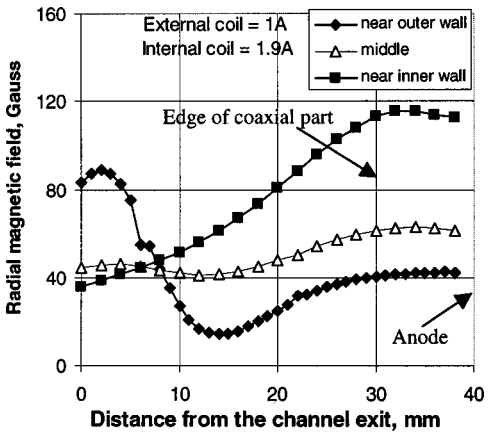

FIG. 4. Radial magnetic field in thruster channel.

ply. Additional voltage regulated and current regulated power supplies were used for the cathode preheating, electromagnetic coil bias and probes.

IV. REVIEW OF HALL THRUSTER DIAGNOSTICS

The distribution of ions outside the thruster is a relatively easy measurement. In our case, the angular ion flux distribution was measured by a flat Langmuir probe rotated from $-90°$ to 90°, along the circle with a radius of 30 cm from the center of the thruster exit. The probe position was measured with a potentiometer. For most operating regimes, the probe characteristics exhibit ion saturation current at a bias voltage of -30 V.[15] The integrated flux distribution gives the total ion current, and the propellant and current utilization. The plume angle is taken to encompass 90% of the total flux.

Integral thruster measurements include dc and ac discharge characteristics, flow rates, and the thrust. Dynamic behavior of the thruster including discharge current and voltage oscillations were monitored by digital PC based oscilloscopes. The thrust was measured with a pendulum type thrust stand, which has a thrust resolution of 0.5 mN.[15] The thruster efficiency, $\eta = T^2/2mP_e$ is deduced from thrust, T, mass flow rate, m, and input power measurements. It is corrected for background pressure, which increases the apparent flow rate by introducing additional gas into the thruster.

The most difficult measurement is the plasma potential inside the thruster. This can be done with cold probes placed along the outer wall of coaxial channel.[16] However, deducing plasma behavior from the near wall potential is complicated by sheath and pre-sheath phenomena.

Alternatively, a movable probe can be immersed inside the thruster.[17–19] The drawback of this technique is strong discharge perturbations induced by the probe, possibly due to ablation of the probe.[19] The discharge current jumps typically to 100%–200% of its magnitude with no probe,[18,19] making it difficult to draw conclusions. However, recently, by reducing the residence time of the probe immersion to about 0.1 s, perturbations of the discharge current have been reduced to less than 15%.[19]

To accommodate a drifting plasma potential, emissive probes can be employed.[20] The probe is typically a hot loop-shaped filament. Strong emission from the filament supplies electrons to the surrounding plasma until a potential difference between disappears. Thus, the ideal floating emissive probe can be a convenient tool to measure the plasma potential with no bias and other difficulties associated with an interpretation of cold probe characteristics.[20,21] However, the difference in the temperatures of the electrons from the hot probe, $T_{ec} < 0.3$ eV and plasma, for Hall thruster $T_{eh} \sim 10-20$ eV, leads to a formation of a double layer, which limits the emission current from the hot floating probe by space charge.[20,22] The floating potential measured by an emissive probe is then still less than the plasma potential, but obviously larger than the floating potential of the cold probe $\Delta\varphi_{fl} = \varphi_p - \varphi_{fl} = 0.5T_e \ln(M_i/2\pi m_e)$. In Ref. 22, considering the case of $T_{ec} \ll T_{eh}$ and taking into account that some of the plasma electrons can penetrate through the double layer to the probe, the ratio between the floating potential of the emitting probe and the electron temperature, $\Delta\varphi_{fl} = 0.95T_{eh}$ was obtained by solving the Poisson's equation with the zero current condition. This solution works well if the magnetic field is normal to the probe surface. However, the magnetic field distribution in Hall thrusters is not uniform and may be oblique or even parallel to the emitting surface.

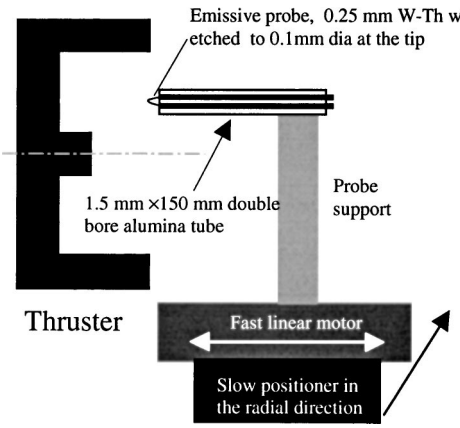

FIG. 5. Schematic of the fast emissive probe setup.

In the experiments described here, we used a fast movable emissive probe to measure the profile of plasma potential inside the thruster (Fig. 5). The emissive probe was fabricated from a 0.25 mm diam thoriated tungsten wire, which was electrolytically etched[23] along about a 5 mm region to a diameter of about 0.1 mm. In addition to a lower work function, thoriated tungsten has a lower evaporation rate than does pure tungsten, something useful for long-time thruster experiments. The probe filament was looped at the place with the small wire diameter. Larger diameter conductor ends were inserted in a double bore alumina tubing of 1.5 mm diameter. The 150 mm length of the tubing allows probe measurements along the whole thruster channel (40 mm), while keeping the main probe setup far away from the thruster exit. The probe heating was by a dc power supply.

The probe tubing is fixed in an aluminum arm connected to the positioner setup. This setup consists of a Normag linear motor with a maximum speed of 1 m/s, assembled on a relatively slow Velmex linear gear motor. The fast positioner provides a fast probe motion in the axial direction, at different radial location maintained by the Velmex motor. The axial position of the probe was measured from the output of its negative feedback sensor with a resolution of 0.05 mm, while the radial location was derived from calibration plots measured at different motor speeds.

Note that $B \sim 0.01-0.015$ T (see Fig. 3), so assuming $\nu_{et} \sim 10^6$ m/s, the electron Larmor radius is larger than 0.1 mm in the whole channel volume, but smaller than 1.5 mm near the inner wall of the coaxial region. Hence, the ceramic tubing may induce plasma perturbations, as it moves through this region. However, employing a thinner probe is made difficult both because of Joule heating and mechanical strength. Results of Ref. 19, conducted at larger magnetic fields and larger plasma densities, but with probes similar in

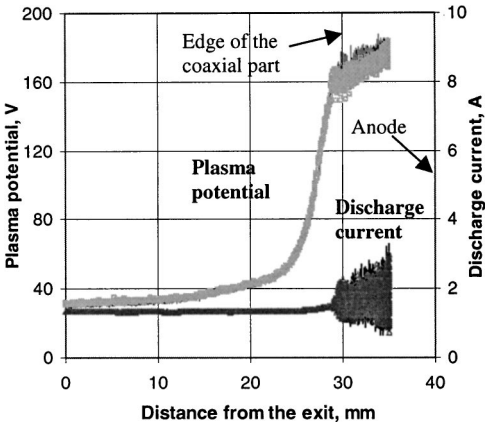

FIG. 6. Plasma potential and discharge current versus probe position along the thruster median. The results were measured in two different sets of probe immersion at a discharge voltage of 200 V and the anode mass flow rate of 1.3 mg/s. Reproducibility of plasma potential measurements is within ±5 V, with the probe in the cylindrical part of the channel. Probe induced perturbations of the discharge current are significant only in the coaxial part of the channel.

sizes, indicated no significant perturbations of the plasma discharge.

The probe potential relative to the cathode, heating power, position output, and discharge current can be monitored simultaneously by a PC-based data acquisition. The total residence time of the probe inside the thruster channel measured with and without thruster operation is less than 0.2 s. In addition, the residence time in the region of a strong magnetic field is 0.1 s. It should be enough to prevent or at least significantly reduce effects associated with probe ablation.[19]

V. EXPERIMENTAL PROCEDURE

The cylindrical Hall thruster was operated in a broad operating regimes: discharge voltage of 100–300 V and flow rates of 10–30 sccm. The procedure of thruster operation and measurements was as follows: After the thruster start-up and thermal steady state (0.5–1 hour), a desired operating regime was maintained by varying the discharge voltage, mass flow rate, and the magnetic field. Then, the thrust, traces of discharge oscillations, and angular ion flux distribution were measured. After that, the fast probe was introduced to the thruster channel, first near its outer wall with no heating and then, with gradually increased heating. At a certain power level, the probe reached saturation values of its floating potentials along the whole travel way. Keeping this power constant, the measurements of plasma potential distribution were repeated a few times to characterize their reproducibility. After that, the heating was gradually turned off and the probe position was changed in the radial direction. In general, at various operating regimes this procedure was repeated in three of four radial positions of the probe.

Figure 6 shows the probe and discharge current behavior versus the probe position measured by a data acquisition system with a sampling rate of 18 000 samples/s at $V_d = 220$ V and mass flow rate of 1.3 mg/s. Here, the radial position of the probe was near the median of the coaxial part of the channel. As can be seen, the use of the fast probe with a reasonable residence time, did not eliminate strong perturbations of the discharge current, which are about 50–100 % of its steady-state value. These perturbations grow rapidly as the probe reaches the region of the coaxial channel with a strong magnetic field. In some probe measurements, as the discharge current approached a current limit of the main power supply, it switched from the voltage regulated to a current regulated mode of operation or oscillated between these two modes. As a result, the applied discharge voltage dropped causing a lower plasma potential measured in the coaxial region (Fig. 7). As the probe is removed from this region back to the cylindrical part of the channel, the power supply usually returned back to a stable voltage regulated mode.

Interestingly, while a ceramic tube without a probe was immersed in the channel, the same amplitude perturbations of the discharge current persisted. Hence, the source of these perturbations may not only be the probe filament emitting electrons.[19] In any event, since probe immersion well inside the cylindrical channel did not produce discharge current perturbations, we will confine our analysis of plasma potential measurements to this particular region.

All potential profiles presented below do not take into account the difference between the measured floating potential of the emissive probe and the plasma potential due to a double sheath effect $\sim 0.95Te$. In addition, the measured potentials have uncertainties due to a voltage drop produced by a dc heating current across the probe filament. As a result, the measured potential includes the potential difference between the probe and a reference electrode and this voltage drop. In the experiments described below, this voltage drop was not larger than 5 V, while at different probe positions in the thruster channel, the total probe potential relative to the cathode was changed from about 30 V–50 V at the thruster exit to almost V_d upstream of the channel.

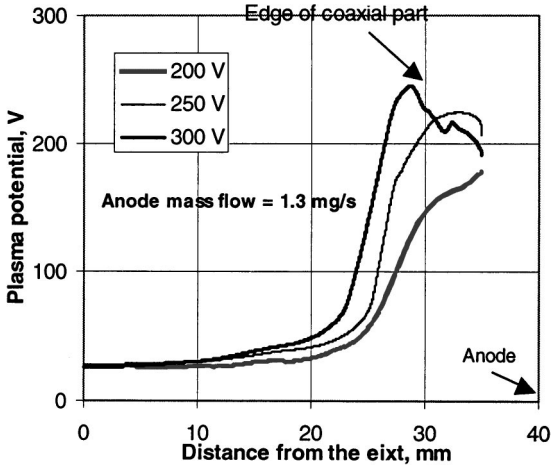

FIG. 7. Plasma potential profiles along the median of the cylindrical thruster at different discharge voltage and xenon mass flow rate of 1.3 mg/s through the anode.

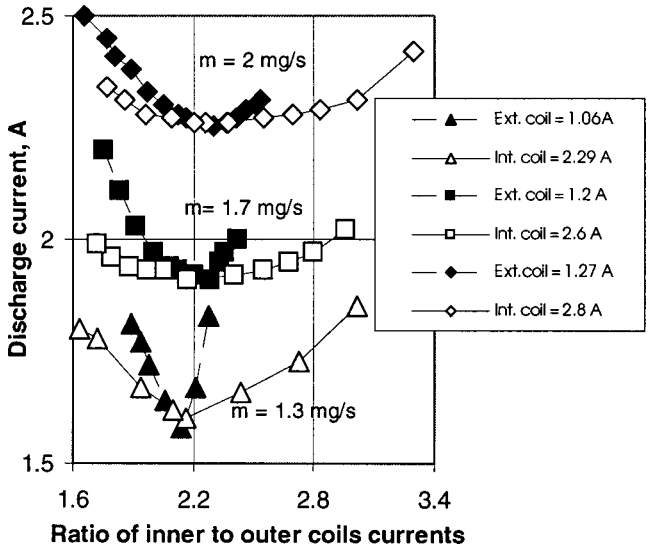

FIG. 8. Discharge current for different magnetic configurations. Current variations in the electromagnet coils, external and internal, change both the magnetic field magnitude and its distribution in the channel.

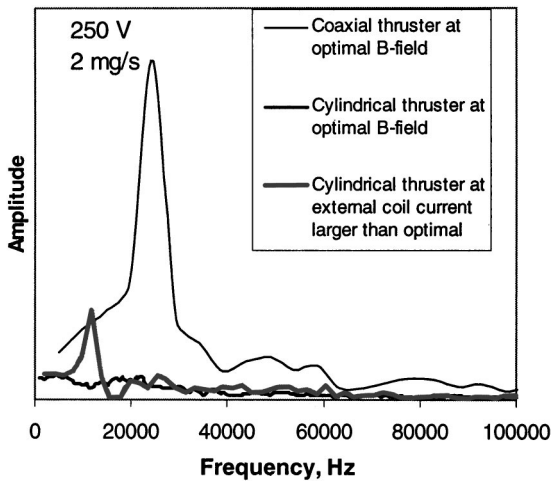

FIG. 9. Spectrum of oscillations in the cylindrical and coaxial Hall thrusters, at a discharge voltage of 250 V and mass flow rate of 2 mg/s.

VI. EXPERIMENTAL RESULTS

Plasma potential profiles are shown in Fig. 7. This representative data was measured by the emissive probe introduced to the channel along the median at different discharge voltages and a constant anode mass flow rate of 1.3 mg/s. The voltage drop is localized mainly to the cylindrical part of the channel where b/L is effectively large. Thus, the ion acceleration mainly takes place in this region. Note that as the discharge voltage is increased, the acceleration region moves towards the thruster exit, but it is still in a strong magnetic field (see Fig. 4). Note that the magnetic field is increased with the discharge voltage, roughly as V_d/B^2, to keep $\lambda_{\text{eff}} \sim$constant. We might speculate that the increase of the discharge voltage increases the electron temperature. Then more ionizing collisions can take place downstream in the thruster channel with an increased magnitude of the magnetic field. The length of the accelerating region is similar to that in conventional thrusters, 1 cm, but the fraction of the voltage drop outside the cylindrical thruster is relatively smaller.[18,19]

Illustrative curves of the discharge current versus the magnetic field at various mass flow rates and at a discharge voltage of 250 V are shown in Fig. 8. Here, by varying the electromagnet coils currents, we changed both the magnetic field and its distribution. Since the magnetic field impedes the axial electron current, the discharge current is lowered by higher magnetic fields. However, above a certain value of the magnetic field, the discharge current increases. In conventional Hall thrusters, this behavior is usually accompanied by growing low frequency discharge oscillations. In Refs. 1 and 24, these oscillations were attributed to ionization instabilities, which appear because of depletion of neutral atoms in the ionization and acceleration region. Their characteristic frequency is roughly as $\nu_a/\lambda_{\text{eff}} \sim 20-30$ kHz.[1]

Interestingly, we did not observe such oscillations in most operating regimes of the cylindrical Hall thrusters. Figure 9 shows examples of spectra measured with coaxial and cylindrical Hall thrusters operated at 250 V and 2 mg/s. Note that the cylindrical thruster is relatively quiet. This surprising result, which is not really understood, may indicate electron transport towards the gas distributor (anode), enhanced in the cylindrical thruster case by the presence of a stronger axial magnetic field. On the other hand, an increase of the current in the external electromagnet coil above its optimal value may still cause low frequency oscillations in the cylindrical thruster. Note that a relatively large peak of these oscillations is at smaller frequencies $\sim$12 kHz (see Fig. 9). We might speculate that the lower frequency of these oscillations here, as opposed to coaxial thrusters, may be attributed to the acceleration region occurring in a wide cylindrical channel with diverging magnetic field lines. As a result, the effective length of the region, which should be filled with neutral atoms, becomes longer.

The effect of the magnetic field on the plasma potential distribution is shown in Fig. 10. The current variations of the external coil affect mainly changes in the potential distribution near the channel walls. In particular, at the external coil current above its optimal value, the voltage potential drop moves towards the anode at the inner wall. As a result, in addition to the axial electric field, there appears a strong radial field. The magnetic field lines, which intersect the anode, should be at the anode potential, pushing the electric field downstream of the channel in the vicinity of the median and the outer wall. Thus, in addition to a strong radial electric field towards the thruster axis, this magnetic field distribution can also lead to the increased discharge current, which was observed at large external coil currents.

In coaxial thrusters with concave magnetic fields, the electron temperature leads to a radial electric field, producing beam divergence. In cylindrical thrusters, the radial electric field is already larger than kT_e/e and so the beam divergence should be large. Figure 11 compares the angular flux distribution measured with coaxial and cylindrical Hall thrusters at 2 mg/s and 250 V. In most of the operating regimes, the half plume angle from the cylindrical thruster is

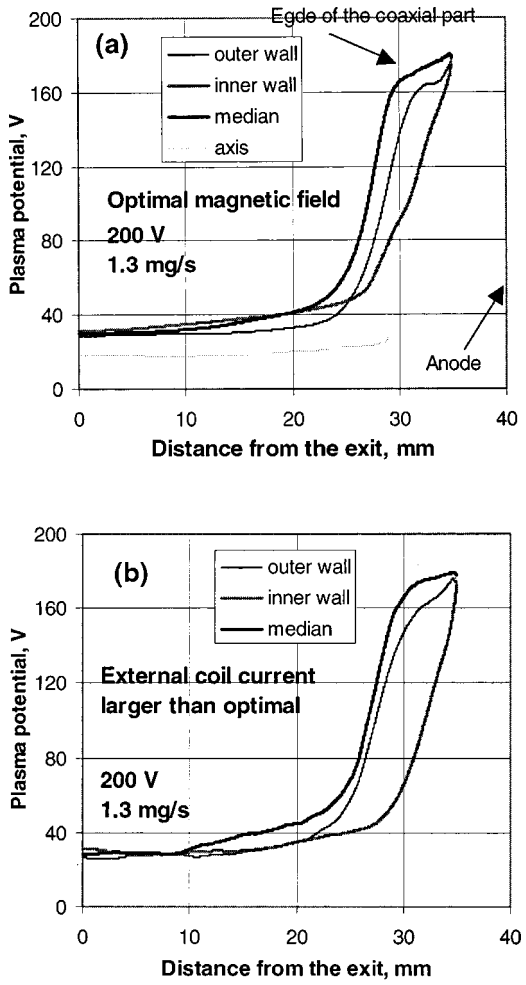

FIG. 10. Plasma potential profiles measured at different magnetic fields: (a) optimal, corresponding to the minimum discharge current; (b) above optimal.

not less than 60°, while in the coaxial thrusters it is typically ~45°–50°.[14,15]

The presence of a strong axial component of the magnetic field may lead to the larger discharge current, compared

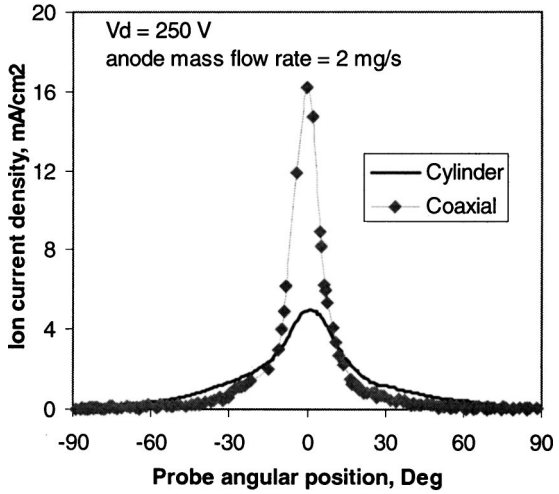

FIG. 11. Comparison of angular ion flux distributions of the cylindrical and coaxial thrusters at 30 cm from the thruster exit.

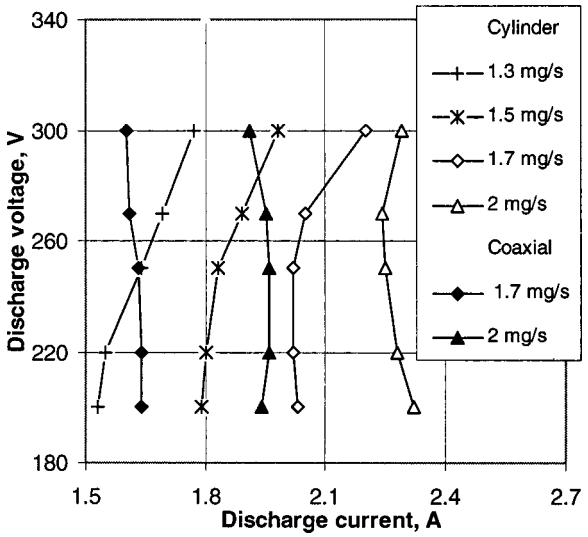

FIG. 12. V–I characteristics of the cylindrical Hall thruster. Note comparison to a 9 cm coaxial Hall thruster at mass flow rates of 1.7 mg/s and 2 mg/s.

to that of coaxial thrusters at the optimal magnetic field. As can be seen in Fig. 12, V–I characteristics of the cylindrical thruster are shifted towards the larger values of the discharge current. At mass flow rates of smaller than 2 mg/s, the discharge current tends to increase with the discharge voltage, while the propellant utilization is almost constant (Fig. 13). Since this increase of the discharge current is accompanied by a reduction of the current utilization efficiency (Fig. 13), it can be attributed to larger electron transport at larger discharge voltages. The poorer propellant and current utilization leads to the lower thruster efficiency of the cylindrical thruster at the anode mass flow rates larger than 1.7 mg/s (Fig. 14).

Interestingly, the cylindrical thruster can operate stable and produce high ion flux at mass flow rates of less than 1.7 mg/s. In these regimes, we did not achieve steady-state operation of the coaxial thruster. Also, although the cylindrical

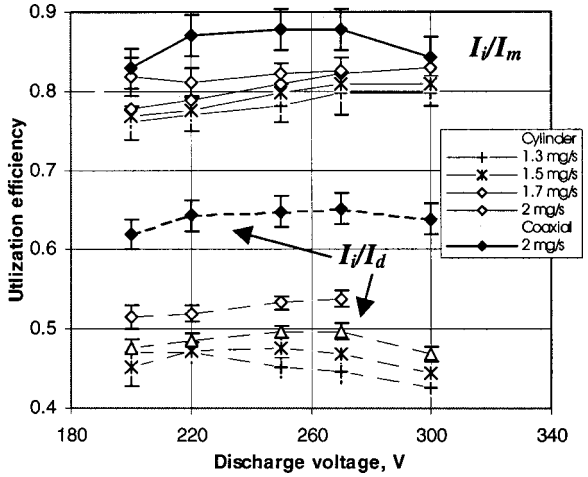

FIG. 13. Propellant utilization, I_i/I_d, and current utilization, I_i/I_d of the cylindrical thruster. Note comparison to the coaxial Hall thruster. The propellant utilization does not include the cathode flow rate of about 0.2 mg/s.

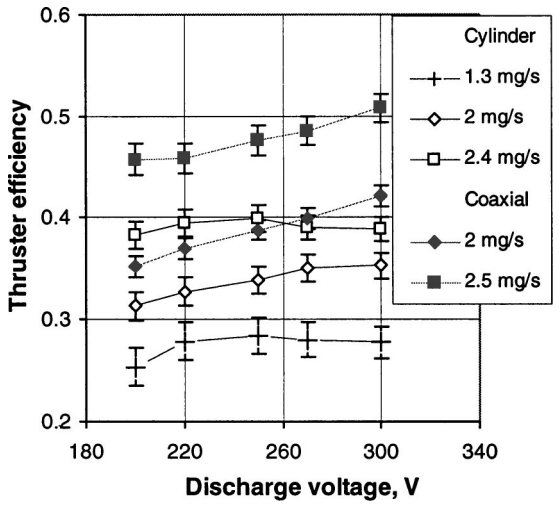

FIG. 14. Thruster efficiency of the cylindrical thruster. Note comparison to the coaxial Hall thruster. The results do not include the cathode flow rate of about 0.2 mg/s.

thruster has larger radial electric field, its propellant utilization is still high. Perhaps, a large b/L ratio and the ''hollow'' anode effect due to the diverging magnetic field in the cylindrical part, allows for more ions to escape from the channel without hitting the walls. Note that these results of the cylindrical thruster were obtained at larger discharge voltages and higher mass flow rates than those reported for end-Hall thrusters of comparable geometry.[10,11]

VII. CONCLUSIONS

Annular conventional Hall thrusters do not scale efficiently to small sizes because of the large surface area to volume and the difficulty in miniaturizing the magnetic circuit. In order to scale the Hall parameter small sizes call for impractical, higher magnetic fields. To overcome difficulties in scaling down, we suggested and studied a Hall thruster with a channel featuring both coaxial and cylindrical regions.

The plasma potential measurements with an emissive floating probe showed that a cusp type of the magnetic field distribution results in a significant accelerating electric field in a quasineutral plasma localized in the cylindrical part of the channel. In this case, the ionization of the propellant atoms remains at a relatively high level and, probably, takes place mainly in the coaxial part of the channel with a smaller channel cross-sectional area. Due to a larger channel height in the cylindrical part, the ions are able to escape from the channel without hitting the walls, producing a large plume angle. The plasma potential distribution and discharge current depend strongly on the magnetic field. The results indicated an optimal magnetic field magnitude and distribution, which should minimize electron transport across the magnetic field. Interestingly, the effect of the magnetic field on the discharge current is not associated with the large amplitude low frequency discharge oscillations, typically observed in coaxial Hall thrusters.

Although, the 9 cm cylindrical thruster is not as efficient as a 9 cm state-of-the-art coaxial thruster, a scaled down cylindrical thruster might be preferred over small coaxial thrusters in which optimization of the magnetic field profile is not feasible. This further scaling is a subject of ongoing research.

ACKNOWLEDGMENTS

The authors thank A. Burlingame, D. Staack, A. Smirnov, K. Ertmer, A. Litvak, and S. Stange for their contribution to this work, and Dr. I. Kaganovich for helpful discussions.

This work was supported by grants from AFOSR and DARPA.

[1] A. I. Morozov and V. V. Savelyev, in *Review of Plasma Physics*, edited by B. B. Kadomtsev and V. D. Shafranov (Consultants Bureau, New York, 2000), Vol. 21, p. 203.
[2] V. V. Zhurin, H. R. Kaufman, and R. S. Robinson, Plasma Sources Sci. Technol. **8**, 1 (1999).
[3] R. Jankovsky, S. Tverdokhlebov, and D. Manzella, AIAA Paper 99-2949, 35th Joint Propulsion Conference, June 1999.
[4] A. V. Zharinov and Yu. S. Popov, Sov. Phys. Tech. Phys. **12**, 208 (1967).
[5] J. Mueller, in *Micropropulsion for Small Spacecraft*, edited by M. M. Micci and A. D. Ketsdever (AIAA Progress in Astronautics and Aeronautics, 2000), Vol. 187, p. 45.
[6] V. Kim, J. Propul. Power **14**, 736 (1998).
[7] Y. Raitses and J. Askenazy, *Proceedings of the XVII International Symposium on Discharges and Electrical Insulation in Vacuum*, Berkeley, CA, 1996.
[8] V. M. Gavryushin and V. Kim, Sov. Phys. Tech. Phys. **26**, 505 (1981).
[9] H. R. Kaufman, R. S. Robinson, and R. I. Seddon, J. Vac. Sci. Technol. **5**, 2081 (1987).
[10] J. Ashkenazy, Y. Raitses, and G. Appelbaum, *Proceedings of the 2nd International Spacecraft Propulsion Conference*, Holland, 1997.
[11] H. R. Kaufman, R. S. Robinson, M. L. Day, and T. W. Haag, AIAA Paper 90-2595, 21st International Electric Propulsion Conference, Orlando, FL, July 1990.
[12] D. R. Shmidt, N. B. Meezan, W. A. Hargus, Jr., and M. A. Capelli, Plasma Sources Sci. Technol. **9**, 68 (2000).
[13] A. Fruchtman, N. J. Fisch, and Y. Raitses, Phys. Plasmas **8**, 1048 (2001).
[14] N. J. Fisch, Y. Raitses, L. A. Dorf, and A. A. Litvak, J. Appl. Phys. (to be published).
[15] Y. Raitses, L. A. Dorf, A. A. Litvak, and N. J. Fisch, J. Appl. Phys. **88**, 1263 (2000).
[16] A. I. Bugrova, A. I. Morozov, and V. K. Kharchevnikov, Sov. Phys. Tech. Phys. **30** (1985).
[17] A. I. Morozov *et al.*, Sov. Phys. Tech. Phys. **17** (1972).
[18] W. A. Hargus, Jr. and M. A. Capelli, AIAA Paper 99-2721, 35th Joint Propulsion Conference, June 1999.
[19] J. M. Haas, and A. D. Gallimore, IEPC Paper 99-078, 26th International Electric Propulsion Conference, Kitakyushu, Japan, October 1999.
[20] N. Hershkowitz, *Plasma Diagnostics: Discharge Parameters and Chemistry* (Academic, New York, 1989), pp. 146–152.
[21] N. Hershkowitz and M. H. Cho, J. Vac. Sci. Technol. **6**, 2054 (1988).
[22] V. A. Rozhansky and L. D. Tsendin, *Transport Phenomena in Partially Ionized Plasma* (Gordon and Breach, Amsterdam, 2000), Chap. 3.
[23] R. W. Motley, J. Appl. Phys. **43**, 3711 (1972).
[24] J. P. Boeuf and L. Garrigues, J. Appl. Phys. **84**, 3541 (1998).